*Korean J. Chem. Eng.*, 33(11), 3184-3193 (2016)
DOI: 10.1007/s11814-016-0178-3

pISSN: 0256-1115
eISSN: 1975-7220

# Fabrication of polysulfone/zinc oxide nanocomposite membrane: Investigation of pore forming agent on fouling behavior

**Shima Javdaneh*, Mohammad Reza Mehrnia*,†, and Maryam Homayoonfal****

*School of Chemical Engineering, College of Engineering, University of Tehran, Tehran, P. O. Box 11155-4563, Iran
**Department of Chemical Engineering, College of Engineering, University of Isfahan, P. O. Box 81746-73441, Isfahan, Iran
(*Received 12 December 2015 • accepted 24 June 2016*)

**Abstract**−The aim of this research was to synthesize a polysulfone/Zinc oxide nanocomposite membrane (PSf/ZnO NCM) in order to mitigate membrane fouling. ZnO nanoparticles with an approximate size of 20 nm were blended with PSf matrix. To fabricate an efficient PSf/ZnO NCM, polyethylene glycol and polyvinyl pyrrolidone were used as pore former agent, based on which PEG-NCMs and PVP-NCMs were fabricated. The effect of the type of pore former and concentration of nanoparticles was evaluated on the structure and performance of nanocomposite membrane. According to SEM images, with the increase in the concentration of nanoparticles, membrane porosity grew as well. AFM analysis confirmed increased roughness with contact angle measurement showing enhanced hydrophilicity. The filtration performance implied that the presence of ZnO nanoparticles improves water flux. Moreover, ZnO nanoparticles elevated humic acid rejection up to 99.7% and 94.2% and decreased total filtration resistance up to 89% and 30% for PEG-NCMs and PVP-NCMs, respectively.

Keywords: Nanocomposite Membrane, ZnO Nanoparticle, Polyethylene Glycol, Poly Vinyl Pyrrolidone, Humic Acid

## INTRODUCTION

Water purification and wastewater treatment have changed into significant environmental issues [1-4]. For industrial and municipal wastewater treatment, biological treatments such as activated sludge and bio filtration have been widely utilized [5]. The membrane bioreactor (MBR) is one of the approaches for this purpose; it is a combination of separation by membrane and employing activated sludge for treatment of water and wastewater [6,7].

The main obstacle in using MBRs is fouling that occurs during filtration, which results in formation of cake in membrane surface, affecting the permeate flux and causing difficulties in operational conditions [8,9]. One of the macromolecules that cause fouling in wastewater treatment systems is humic acid. Humic acid (HA) is a mixture of natural organic macromolecules that has a range of physicochemical properties and exhibits different activities across environmental systems [10]. Due to the presence of different functional groups in HA structure like COOH, OH and COH, this molecule tends to attach and deposit on surfaces and other molecules [11]. In addition to membrane fouling, the presence of humic acid attached to chlorine, ozone, chlorine dioxide and chloramines molecules produces an undesirable and potentially harmful disinfection by-product [11-13]. Humic acid can react with chlorine to create carcinogenic compounds and also form different complexes with heavy metals [14,15]. It has also been reported that the interaction of humic acid can be harmful for human red blood cells. Further, discharge of humic acid through industrial sewage may cause soil erosion and damage marine water life [16]. High concentrations of humic acid exist in raw wastewater as well as in primary, secondary and tertiary effluents of municipal wastewater treatment systems [17,18]. In addition, studies have noted that humic acid is used as a model molecule to investigate the fouling behavior of membrane in wastewater treatment application [15,19,20]. Accordingly, recognition of humic acid compounds in different steps of wastewater and water treatment and also the fouling behavior of the compounds is extremely important.

Based on the hydrophobic nature of polymeric membranes, hydrophobic materials attach to the surface of membrane during filtration process in MBRs; therefore, different routes have been applied for mitigation of hydrophobicity of polymeric membranes to avoid fouling. There are various methods to achieve this aim [21]. All of these methods are based on increasing hydrophilicity of the whole membrane or the surface of membrane. In recent years, applying nanoparticles, especially metal oxide nanoparticles, has attracted a great deal of attention among other existing methods [22, 23]. A nanocomposite membrane which contains regular distribution of nanoparticles in the casting solution and thus in polymeric film brings about enhancement of hydrophilicity of membrane and consequently decreased membrane fouling [24]. Among various metal oxide nanoparticles, zinc oxide nanoparticles have attractive properties such as hydrophilicity, photo catalytic activity and antibacterial properties which have attracted a great deal of attention among recent studies [23]. Different studies have been carried out on humic acid filtration using nanocomposite membranes. Yunos et al. used 18 wt% PSF, PEG, 2, 4, 6-triaminopyrimidine (TAP) as compatibilizer, ZnO nanoparticles and NMP for humic acid filtration. The results showed developed flux and rejection levels [25]. Leo et al. synthesized PSF/ZnO nanocomposite membrane with

†To whom correspondence should be addressed.
E-mail: mmehrnia@ut.ac.ir

**Table 1. Composition of synthesised membranes**

| No. | Membrane type | PSF% | NMP% | PEG% | PVP% | (ZnO/PSF)% |
|---|---|---|---|---|---|---|
| 1 | PEG-blank | 16 | 75 | 9 | - | 0 |
| 2 | PEG-NCM0.3 | 16 | 75 | 9 | - | 0.3 |
| 3 | PEG-NCM0.5 | 16 | 75 | 9 | - | 0.5 |
| 4 | PEG-NCM0.6 | 16 | 75 | 9 | - | 0.6 |
| 5 | PEG-NCM1 | 16 | 75 | 9 | - | 1 |
| 6 | PEG-NCM1.5 | 16 | 75 | 9 | - | 1.5 |
| 7 | PEG-NCM2 | 16 | 75 | 9 | - | 2 |
| 8 | PVP-blank | 16 | 79 | - | 5 | 0 |
| 9 | PVP-NCM0.3 | 16 | 79 | - | 5 | 0.3 |
| 10 | PVP-NCM0.5 | 16 | 79 | - | 5 | 0.5 |
| 11 | PVP-NCM0.6 | 16 | 79 | - | 5 | 0.6 |
| 12 | PVP-NCM1 | 16 | 79 | - | 5 | 1 |
| 13 | PVP-NCM1.5 | 16 | 79 | - | 5 | 1.5 |

poly vinyl alcohol (PVA) to reduce fouling of oleic acid. Nanocomposite membrane with 2 wt% of ZnO nanoparticles exhibited less reduction in flux in comparison with PSF membrane without nanoparticles [26]. Balta et al. used ZnO nanoparticles in polyethersulfune and found that nanocomposite membranes had lower flux decline compared to neat polymeric membranes. In addition, rejection of methylene blue increased from 47.5% for neat membrane to 82.3% for blended membranes [23]. Ahmad et al. synthesized ZnO nanocomposite membrane by 15.75 wt% PES as polymer and PVP as pore former for filtration of humic acid. The optimum concentration of nanoparticles was 1.25 wt% offering a pure water flux of about 317.45 LMH [15]. In these studies, different compositions and percentages of materials were used, leading to different weight percentage of ZnO nanoparticles and amount of flux.

In this study, since the efficiency of ZnO nanoparticle depends on its arrangement around membrane pores, two different pore former agents, PEG and PVP, were examined. Based on surface properties, structural morphology and filtration performance, the optimum membrane structure with a low filtration resistance was introduced. Finally, the impact of zinc oxide nanoparticles on hydrophilicity, pure water flux, HA flux and the polysulfone membrane fouling behaviour was studied.

## MATERIALS AND METHODS

### 1. Materials

BASF Polysulfone (PSF) as the main polymer matrix was supplied by Ultrason. N-methylene-2-pyrrolidone (NMP) was provided by Merck and used as a solvent. Poly (ethylene glycol) (PEG) and poly (vinyl pyrrolidone) (PVP) with respective average molecular weights of 20000 and 29000 were purchased from Merck and Sigma Aldrich, respectively, and used as pore former. ZnO nanoparticles (20 nm) synthesized via wet chemical method, were purchased from Research Institute of Petroleum Industry, Iran. Humic acid powder and NaOH pellets were purchased from Sigma Aldrich and Merck, respectively.

### 2. Membrane Synthesis

Nanoparticles with an average size of 20 nm were dispersed in NMP by an ultrasonic bath (Elmasonic S 30H) for about 2 hours in 70 °C. Then polysulfone films containing ZnO nanoparticles were synthesized via phase inversion method. The details on film fabrication have been reported previously [27].

In the first step, the first type of nanocomposite polysulfone membranes was synthesized with PEG as a pore former agent. In the composition of this type, NMP and PEG 20000 were used as a solvent and pore former, and polysulfone 16 wt% as polymer was utilized. Concentrations of ZnO nanoparticles were 0.3, 0.5, 0.6, 1, 1.5 and 2 wt% of polymer.

In the second step, the second type of nanocmposite membrane was fabricated with PVP as a pore former. Polysulfide 16 wt% was used in the composition of membrane, NMP as a solvent and PVP 29000 as a pore former. ZnO nanoparticles were used as much as 0.3, 0.5, 0.6, 1 and 1.5 wt% of polymer in this nanocomposite membrane. The name and composition of fabricated membranes are provided in Table 1. To name a membrane, the abbreviation of the pore former comes first, followed by NCM as the abbreviation of nanocomposite membrane and eventually comes the weight percentage of ZnO nanoparticle. Note that PEG-blank and PVP-blank are membranes without nanoparticles.

### 3. Membrane Characterization and Evaluation of the Performance

The structure and functionality of synthesized nanocomposite membranes containing PEG or PVP pore former were assessed. The morphology and surface properties of the synthesized membranes were evaluated using SEM and AFM analysis, calculation of porosity and pore size, and contact angle measurement. Thereafter, the filtration performance of the synthesized nanocomposite membrane was compared in terms of pure water flux, humic acid rejection and membrane filtration resistance.

3-1. Scanning Electron Microscopy (SEM) Analysis

To observe the presence of nanoparticles and structural form of membranes and pores, SEM images were taken by Hitachi, S-4160 apparatus, Japan. So as to see the cross-section, membrane samples were broken by liquid nitrogen. All of the samples were dried, then covered with a thin gold layer to make them conductive and prepared to be observed by SEM. The effect of the amount of ZnO

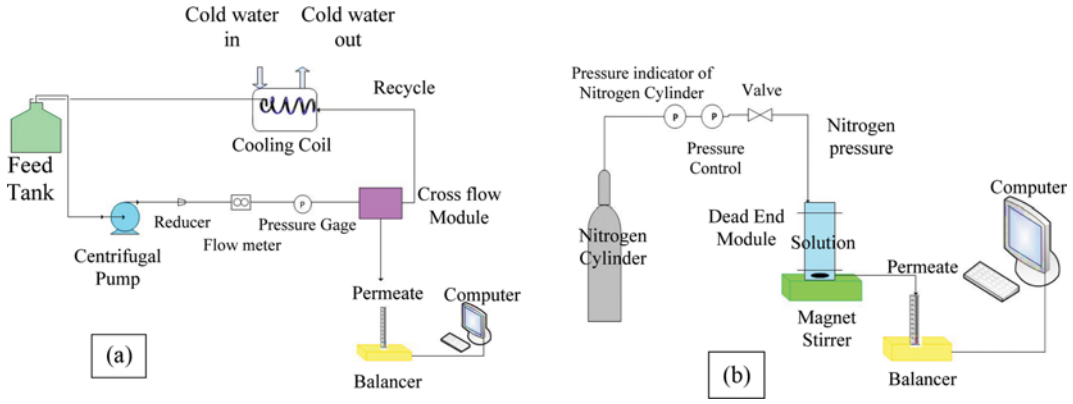


**Fig. 1. The Schema of Cross flow (a) and Dead end (b) filtration systems.**

nanoparticles and the pore former type was investigated through the obtained images.

3-2. Atomic Force Microscopy (AFM) Analysis

AFM test was employed to investigate the changes in the morphology and roughness of the surface of membranes synthesized under various conditions. The parameter of roughness is important in membrane fouling, which is among the properties of the membrane itself and measurable by AFM images. AFM images were also taken by Veeco machine in 2 Hz and 256*256 resolutions, to investigate the membrane roughness. RMS roughness for membranes was calculated based on equations presented in our previous studies [24,28].

3-3. Contact Angle Analysis

Contact angle measurements were performed for analyzing the hydrophilicity of membranes. The angle between water droplet and membrane was recorded by Canon EOS 50D+EF 100 mm f/2.8L Macro IS USM and then calculated by ImageJ software [29,30]. The porosity of membranes and mean pore size were calculated by dry-wet weight [31] and filtration velocity [32,33] methods, respectively [4].

3-4. Pore Size and Porosity Measurement

To calculate the porosity of synthesized membranes, each membrane was cut into a specific size and then immersed in distilled water for one day. After that, the water on the surface of the membranes was wiped carefully by a clean tissue and the membranes were weighed ($W_w$). Then the membranes were dried for one day in a desiccator and weighed again ($W_d$). The porosity of membrane was calculated through the equation presented in the equation section. The mean pore radius was determined by Guerout-Elforl-Ferry equation [34] presented as Eq. (2) in the equations section.

$$\varepsilon = \frac{W_w - W_d}{\rho_w \times V} \tag{1}$$

$$r_p = \sqrt{\frac{(2.9 - 1.75\varepsilon) \times 8\eta l Q}{\varepsilon \times A \times \Delta P}} \tag{2}$$

## 4. Evaluation of the Membrane Filtration Performance

To evaluate the membrane performance, both cross flow and dead-end filtration set-ups were used, since each one had a specefic advantage at some stage. Membrane fouling experiments are dead-end experiments [35,36], whereas membrane filtration in practice is carried out in a cross-flow mode [37].

Therefore, the membrane resistance and fouling in humic acid filtration were evaluated (including initial pure water flux, the final pure water flux, flux of humic acid solution measurement) by a dead-end filtration system equipped with a stirrer for preventing concentration polarization with a filtration area of 4.52 $cm^2$ at 25 °C and pressure of 3 bars. This was because of its low feed volume (100 mL) without recycling which limited loss of humic acid solution during filtration [23,38].

On the other hand, since for industrial applications, a cross-flow operation is preferred because of the lower fouling tendency relative to the dead-end mode [37], the membrane pure water flux was evaluated in a crossflow system with a filtration area of 21 $cm^2$ at 25 °C and pressure of 3 bars. This system was chosen due to its high feed volume (15 L), feed recycling, and consequently its applicability in long time runs.

A schema of experimental cross-flow and dead-end set ups is demonstrated in Fig. 1. Permeate was collected and weighed by digital balance which was connected to a computer for recording permeate weight for every one-tenth of a second and then was converted to flux. In both systems, the stabilization period for membrane compaction was 15 minutes and unsteady state period was 30 to 45 minutes, after which data was recorded.

The permeate flux was calculated using Eq. (3) and fouling of membrane was calculated using the serial resistance model [15] through Eqs. (4) to (8) presented in the equations section.

$$J_p = \frac{V_p}{A \times \Delta t} \tag{3}$$

$$J = \frac{\Delta P_T}{\mu R_t} \tag{4}$$

$$R_t = R_m + R_c + R_p \tag{5}$$

$$R_m = \frac{\Delta P_T}{\mu J_{w1}} \tag{6}$$

$$R_p = \frac{\Delta P_T}{\mu J_{w2}} - R_m \tag{7}$$

$$R_c = \frac{\Delta P_T}{\mu J_s} - R_m - R_P \quad (8)$$

Total filtration resistance, $R_t$ ($m^{-1}$) consists of membrane resistance ($R_m$), cake resistance ($R_c$) and fouling resistance in pores, which is irreversible for the absorption of substances onto pore walls and membrane surface ($R_p$). For measurement of $R_p$, the cake layer was physically removed from the membrane surface, followed by rinsing the membrane surfaces by deionized water for 10 minutes [15].

Since humic acid dissolves in alkaline solutions, for preparation of 25 ppm of the desired solution, a suitable quantity of humic acid powder was dissolved in NaOH 0.1 N solution. The HA rejection experiment was calculated based on Eq. (9) presented in the equations section. The concentration of humic acid in the permeate solution was measured using UV spectrophotometer (Unico 2100 Spectrophotometer) at a wavelength of 254 nm [15].

$$\text{HA Rejection (\%)} = \left(1 - \frac{C_P}{C_f}\right) \times 100 \quad (9)$$

## RESULTS AND DISCUSSION

The structure and functionality of the synthesized nanocomposite membranes containing PEG or PVP pore former were assessed. The morphology and surface properties of the synthesized membranes were evaluated through SEM and AFM analysis, porosity and pore size calculation and contact angle measurement. Thereafter, the filtration performance of the synthesized nanocomposite membrane was compared with that of the blank membrane in terms of pure water flux, humic acid rejection and membrane filtration resistance.

### 1. Scanning Electron Microscopy (SEM) Analysis

The cross-sectional SEM images of PEG-NCM and PVP-NCM membranes containing different concentrations of ZnO nanoparticle are presented in Figs. 2 and 3, respectively. The processed SEM images are also presented showing skin layer thickness and membrane pores (the right images in Figs. 2 and 3). As can be seen, larger quantities of ZnO nanoparticles to the casting solution of PEG-NCM and PVP-NCM membranes cause an increase in the size of

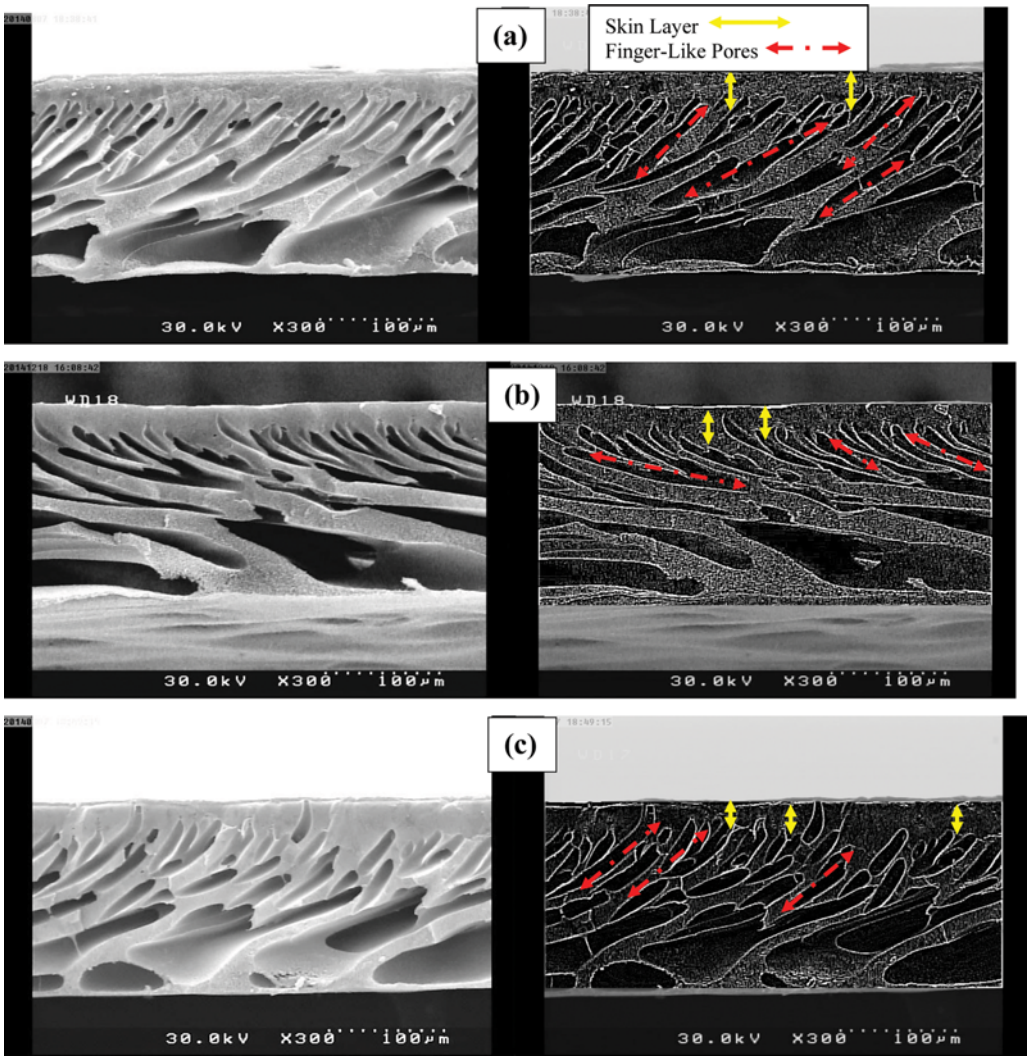


**Fig. 2. Coss-sectional SEM images (left) of PEG-blank (a), PEG-NCM0.5 (b), PEG-NCM2 (c) membranes and processed SEM images (right) showing skin layer and finger-like pores.**

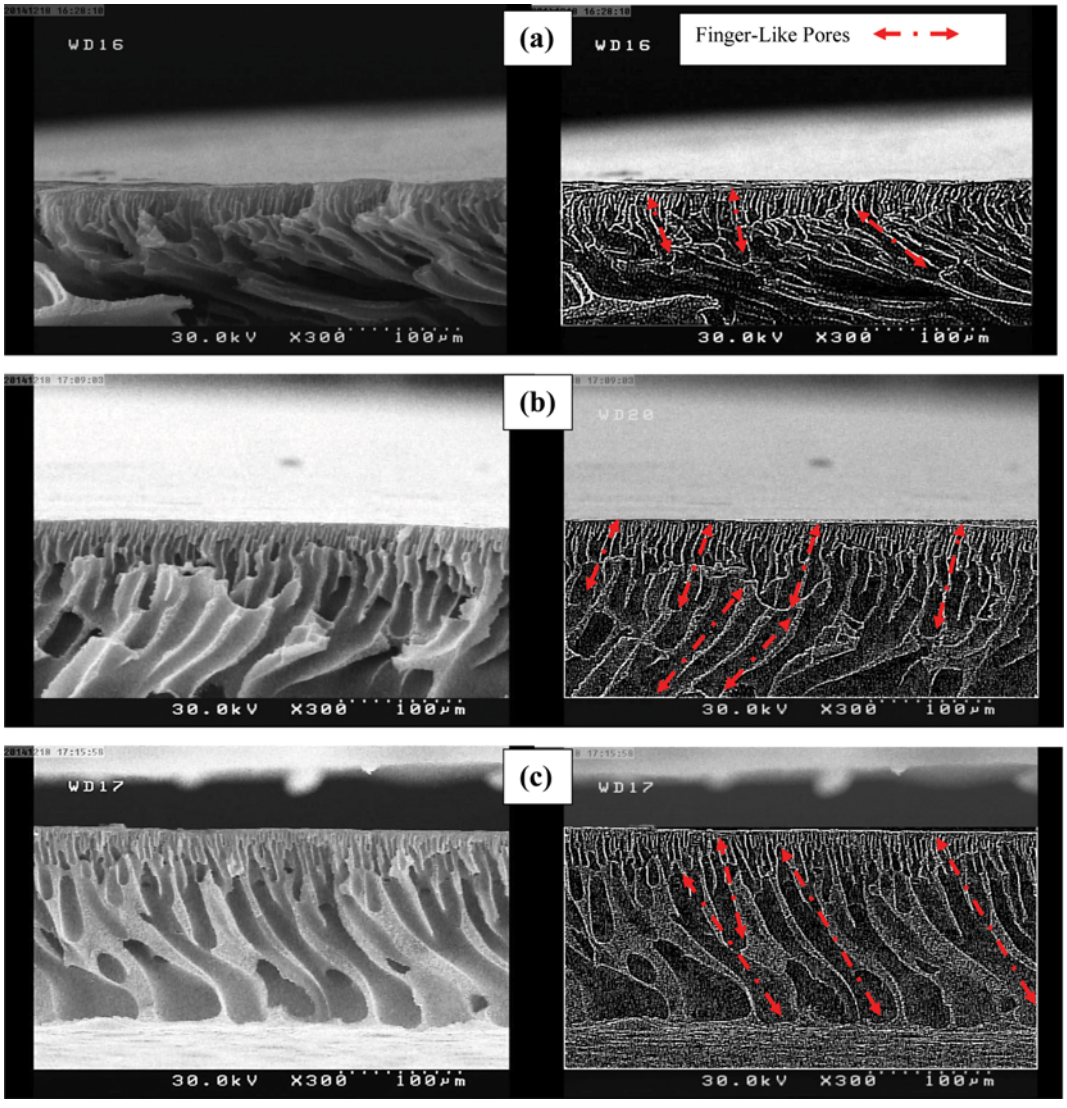


**Fig. 3. Coss-sectional SEM images (left) of PVP-blank (a), PVP-NCM0.3 (b), PVP-NCM1.5 (c) membranes and processed SEM images (right) showing finger-like pores.**

finger-like pores and a decrease in thickness of dense layer on membrane surface. Changes in the structure of pores, which is due to the increased number of ZnO nanoparticles in the casting solution, could be an outcome of changes that have been made in the phase inversion speed. Indeed, the tendency of hydrophilic ZnO nanoparticles to the hydrophilic non-solvent bath (water) has caused enhanced phase separation speed, hence instantaneous phase separation occurs and more porous structures are created [24].

Moreover, based on the structural comparison of PEG-NCM and PVP-NCM type nanocomposite membranes in Figs. 2 and 3, it is concluded that the skin layer of PEG-NCMs is thicker than PVP-NCM's. This can be related to the difference in the speed of phase inversion process during formation of these two types of membranes. Han and Nam showed that at low PVP concentrations (below 20 wt%), instant demixing occurred and contributed to enlargement of membrane pores, thinness of the membrane top layer. In contrast, for high PVP concentrations (more than 20 wt%), delayed demixing occurred due to the increase in the polymer solution viscosity, suppressing the macro-void formation in the membrane structure [39]. For the membrane using PEG as pore former, Panda and De showed that macro-void formation increases and the top layer thickness diminishes from 0 wt% of PEG to 5 wt% of PEG, followed by reduction in the macro-void formation and elevation of the top layer thickness [40]. This is the reason why PVP-NCMs have a thin top layer and more finger like pores with less width, while PEG-NCMs have a thicker skin layer and fewer finger like pores with a larger width.

**2. Atomic Force Microscopy (AFM) Analysis**

Three-dimensional AFM images of both PEG-NCM and PVP-NCM are provided in Fig. 4.

Based on Fig. 4, the more nanoparticles are used in the casting solution, the higher the roughness is. This happens because of hydrophilicity of nanoparticles and their tendency to remain in the coagulation bath [41,42]. For better explanation, the RMS (root mean square) roughness of the synthesized membranes is presented in Table 2. In addition, the RMS roughness of some ZnO-containing

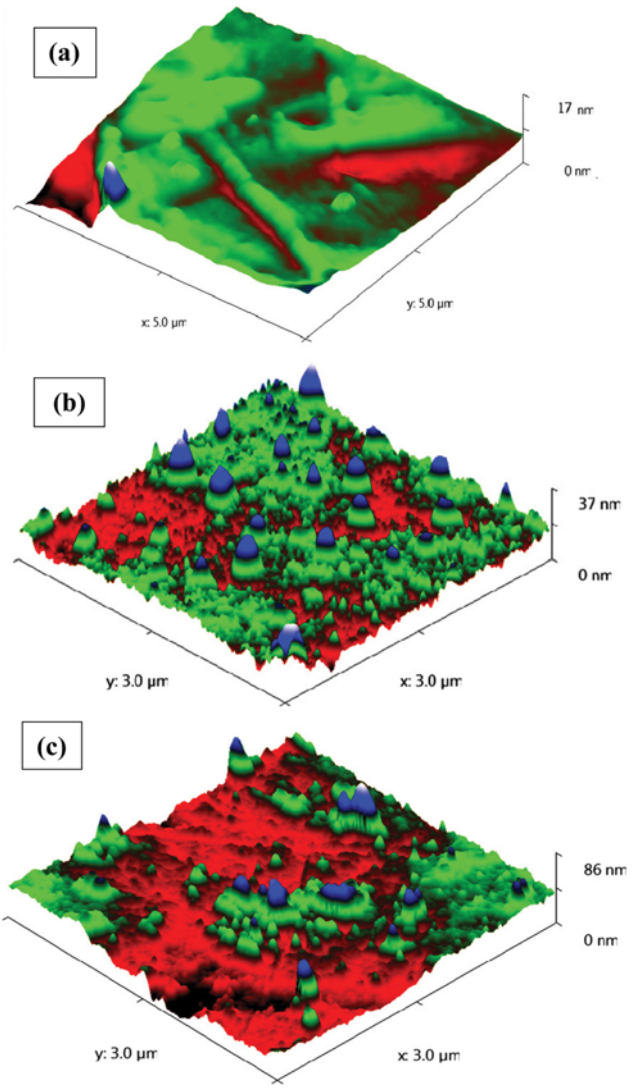


**Fig. 4. AFM images of PEG-blank membrane (a), PEG-NCM0.5 (b) and PEG-NCM2 (c) nanocomposite membranes.**

nanocomposite membranes, which has been reported recently [25,43-45], is included for further comparison.

As presented in Table 2, by raising ZnO nanoparticles from 0 to 2 wt%, RMS roughness increases from 11 to 61 nm in accordance with other studies [15,25]. As implied in the presented data, the effect of ZnO loading on the roughness enhancement in this research is more noticeable than in other presented research. This could be due to delayed demixing of PEG-NCMs casting solution and giving enough time to nanoparticles to move towards the membrane surface and make the membrane surface rougher.

**3. Contact Angle Measurement**

To evaluate the of membrane surface hydrophilicity, contact angle analysis was done. According to Table 3, in synthesized nanocomposite membranes, the more nanoparticles were used, the less the contact angle was. For PEG-NCM membranes, by 2 wt% increase in nanoparticle concentrations, 40% decrease was observed in contact angle. For PVP-NCMs 11.6% reduction in contact angle was reported for PVP-NCM1.5.

It can be concluded that the effect of nanoparticle loading on hydrophilicity enhancement of PEG-NCM membranes is more noticeable than for PVP-NCM membranes. Indeed, during the phase inversion process, ZnO nanoparticles tend to be in coagulation bath because of their hydrophilic nature. Therefore, the largest population of nanoparticles is present in the membrane skin layer [28]. For PVP-NCMs, phase inversion occurs instantly [46]; therefore nanoparticles do have enough opportunity to move towards membrane surface, resulting in less effectiveness of ZnO nanoparticle loading on membrane surface hydrophilicity in comparison with PEG-NCMs with delay demixing.

**4. Pore Size and Porosity Measurement**

The average porosity and mean pore size of different nanocomposite membranes were calculated are presented in Table 4. As a clearer explanation on the size of pores, it was proven that ZnO nanoparticle loading had no significant effect on PEG-NCM membrane pore size, but for PVP-NCM all nanocomposite membranes had a larger pore size than PVP-blank. In PEG-NCM type, all nanocomposite membranes were more porous than PEG-blank, and for PVP-NCM the porosity increased for the membrane that contained 1 wt% ZnO, after which the porosity declined. As a result, the porosity of PEG type membrane increased up to 30%, while for PVP-NCM type 5% enhancement was observed. This trend was also observed in cross-sectional SEM images (Fig. 2) in which a conspicuous increase in the porosity of PEG-NCM membranes occurred by ZnO nanoparticle loading. This is because of delayed demixing of PEG-NCMs during which nanoparticles can act as promoter agent and speed up the phase inversion and make membrane more porous. In contrast, for PVP-NCM because of instant demixing of casting solution, the effect of nanoparticles on demixing promotion is less obvious.

**5. Filtration Performance**

The filtration performance of all synthesised nanocomposite membranes was evaluated in terms of pure water flux, membrane resistance, and humic acid rejection. Pure water flux of PEG-NCM evaluated in both cross-flow and dead-end modules is presented in Fig. 5. It confirms that for all membranes regardless of the nanoparticle dosage, pure water flux measured in dead end module is larger than in their cross-flow counterparts. Indeed, in the dead-end filtration the feed flow is perpendicular to the membrane surface so in a similar pressure, dead end module shows higher permeate flux than cross flow system [37].

Fig. 5 also indicates that by adding nanoparticles to the casting solution up to 0.5 wt%, the pure water flux increased in both cross-flow and dead-end modules. This occurred because of the formation of larger pores (see SEM images in Fig. 2) and enhanced hydrophilicity (see Table 3) as well as the increment in porosity (see Table 4) for PEG-NCM0.5. Flux elevation is also a result of great distribution of nanoparticles in the casting solution leading to increased hydrophilicity [21]. AFM images also demonstrated greater roughness as more nanoparticles were used; therefore, the area for water to diffuse into the membrane increased and affected the flux pattern [25]. Flux decrement after threshold limit (0.5 wt%,) is due to aggregation of nanoparticles in pores and viscosity increment of casting solution resulting in prolongation of coagulation process and formation of pores with a small size [42]. The calculation of

**Table 2. RMS roughness of synthesised nanocomposite membranes along with RMS roughness reported in literatures for ZnO containing nanocomposite membranes**

| No. | Composition | Membrane name | ZnO wt% | RMS Roughness (nm) | Reference |
|---|---|---|---|---|---|
| 1 | PSF/PEG/ZnO | PEG-blank | 0 | 11 | This study |
| | | PEG-NCM0.5 | 0.5 | 30 | |
| | | PEG-NCM2 | 2 | 61 | |
| 2 | PSF/PEG/TAP/ZnO | 1 | 0 | 18.56 | Yunos et al. [25] |
| | | 2 | 0.5 | 24.91 | |
| | | 3 | 2 | 30.21 | |
| 3 | PSF/ZnO | Pure PSu | 0 | 15.1 | Alhoshan et al. [47] |
| | | 0.1 wt% PSu/ZnO | 0.1 | 16 | |
| | | 0.2 wt% PSu/ZnO | 0.2 | 23 | |
| 4 | PSF/ZnO | PSf-0 | 0 | 92.92 | Moradihamedani et al. [48] |
| | | PSf-0.1 | 0.1 | 80.31 | |
| | | PSf-1 | 1 | 72.51 | |
| | | PSf-3 | 3 | 174.50 | |
| | | PSf-5 | 5 | 195.20 | |
| 5 | PSF/ZnO | Pristine PSF | 0 | 25 | Gaur et al. [49] |
| | | 3 mass% ZnO/PSF | 3 | 10 | |
| | | 5 mass% ZnO/PSF | 5 | 14 | |
| | | 10 mass% ZnO/ PSF | 10 | 85 | |

**Table 3. Cotact angle contents of synthesized membranes**

| Membrane | Contact angel content |
|---|---|
| PEG-blank | 69 |
| PEG-NCM0.3 | 66 |
| PEG-NCM0.5 | 55 |
| PEG-NCM0.6 | 55 |
| PEG-NCM1 | 51 |
| PEG-NCM1.5 | 45 |
| PEG-NCM2 | 40 |
| PVP-blank | 77 |
| PVP-NCM0.3 | 75 |
| PVP-NCM0.5 | 73 |
| PVP-NCM0.6 | 71 |
| PVP-NCM1 | 71 |
| PVP-NCM1.5 | 68 |

**Table 4. Average porosity and mean pore radius of synthesized membranes**

| Membrane | $\varepsilon_{average}$ | Mean pore radius (nm) |
|---|---|---|
| PEG-blank | 0.399 | 64.96 |
| PEG-NCM0.3 | 0.526 | 55.94 |
| PEG-NCM0.5 | 0.532 | 65.58 |
| PEG-NCM0.6 | 0.40 | 78.09 |
| PEG-NCM1 | 0.51 | 65.65 |
| PEG-NCM1.5 | 0.445 | 58.89 |
| PEG-NCM2 | 0.413 | 69.27 |
| PVP-balnk | 0.44 | 47.29 |
| PVP-NCM0.3 | 0.464 | 50.46 |
| PVP-NCM0.5 | 0.458 | 49.77 |
| PVP-NCM0.6 | 0.468 | 49.77 |
| PVP-NCM1 | 0.368 | 53.88 |
| PVP-NCM1.5 | 0.43 | 52.62 |

porosity also proved that PEG-NCM0.5 is the most porous nanocomposite membrane which, based on Fig. 5, showed 51% enhancement in pure water flux in comparison to PEG-blank.

Pure water flux of PVP-NCM evaluated in both cross-flow and dead-end modules is shown in Fig. 6 which as with PEG-NCM shows greater water flux for dead-end module rather than the cross-flow system.

In Fig. 6 PVP-NCM0.3 and PVP-NCM1.5 show a better pure water flux with 22% enhancement rather when compard with PVP-blank. In comparison of PVP and PEG type membranes, because there is greater polymeric propertyin PVP than PEG, the flux of PVP type membranes is lower than PEG type counterparts. SEM images presented in Figs. 2 and 3 also confirm the higher porosity of PEG-NCMs rather than PVP-NCM. This can be due to solvent-nonsolvent exchange rate during phase inversion and formation of little pores in PVP-NCM type membrane [47].

The filtration resistance of humic acid by PEG-NCMs is represented in Table 5. In general, all synthesized nanocomposite membranes have a lower filtration resistance compared to the blank ones. According to Table 5, PEG-NCM0.5, as expected from pure water flux data in Fig. 5, has the lowest membrane resistance ($R_m$); therefore, this nanocomposite membrane has the best performance in water filtration. Considering other filtration resistances, PEG-NCM1.5 with 89%, 95% and 75% decrease in total, cake and pore resistances respectively, have the best performance. It seems that even though PEG-NCM1.5 has a lower pure water flux than PEG-

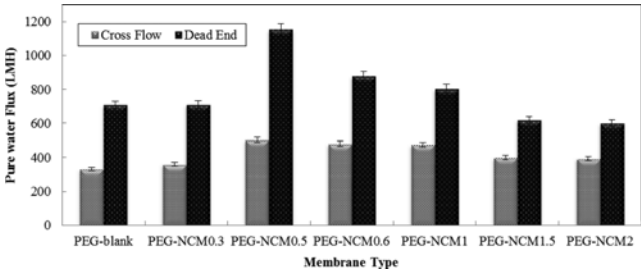


**Fig. 5. Pure water flux of PEG-NCM membranes in both cross-flow and dead-end modules.**

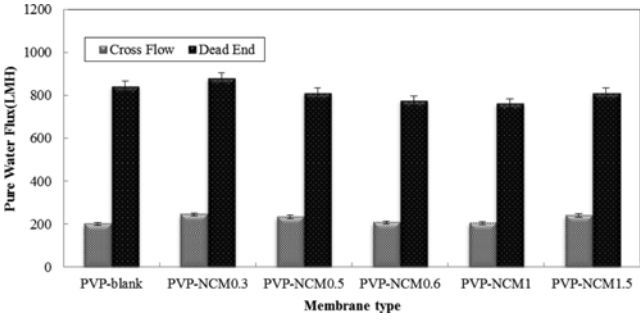


**Fig. 6. Pure water flux of PVP-NCM membranes in both cross-flow and dead-end modules.**

**Table 5. Humic acid filtration resistance for PEG-NCM type nanocomposite membranes**

| $R_t*10^{11}$ ($m^{-1}$) | $R_C*10^{11}$ ($m^{-1}$) | $R_P*10^{11}$ ($m^{-1}$) | $R_m*10^{11}$ ($m^{-1}$) | Membrane type |
|---|---|---|---|---|
| 303.25 | 237.33 | 48.79 | 17.13 | PEG-blank |
| 284.96 | 235.91 | 32.71 | 16.34 | PEG-NCM0.3 |
| 35.99 | 13.19 | 12.28 | 10.52 | PEG-NCM0.5 |
| 29.58 | 5.32 | 4.7 | 19.56 | PEG-NCM1.5 |
| 131.84 | 64.8 | 7.11 | 60.65 | PEG-NCM2 |

**Table 6. Humic acid filtration resistance for PVP-NCM type nanocomposite membranes**

| $R_t*10^{11}$ ($m^{-1}$) | $R_C*10^{11}$ ($m^{-1}$) | $R_P*10^{11}$ ($m^{-1}$) | $R_m*10^{11}$ ($m^{-1}$) | Membrane type |
|---|---|---|---|---|
| 31.92 | 3.04 | 14.61 | 14.27 | PVP-blank |
| 45.77 | 10.3 | 21.73 | 12.14 | PVP-NCM0.3 |
| 67.38 | 9.62 | 7.64 | 50.12 | PVP-NCM0.5 |
| 22.46 | 2.9 | 7.43 | 12.13 | PVP-NCM1.5 |

NCM0.5, the presence of three times more ZnO nanoparticles in its matrix makes this membrane have a better filtration performance in terms of resistance. In general, considering membrane resistance PEG-NCM0.5 is the best membrane, while considering total, cake and pore resistance, PEG-NCM1.5 is the best membrane.

Considering the data presented in Tables 5 and 6, it is important to mention that with a specific amount of increase in ZnO nanoparticle loading, the membrane cake resistance increases, which can be related to membrane surface roughness [24], as shown in Fig. 4 and Table 2; it indicates that the surface under the membrane has a good potential for attachment of substance onto it.

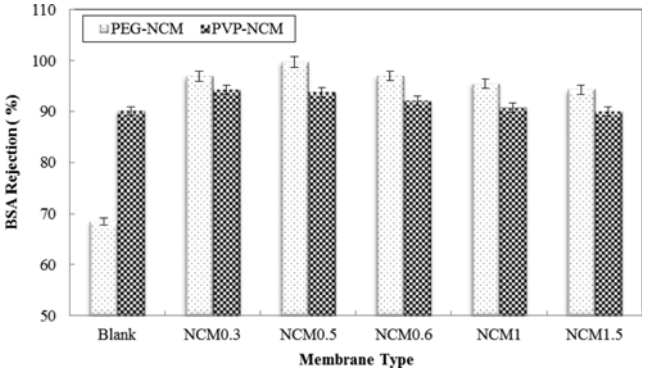


**Fig. 7. Humic acid rejection of PEG-NCMs and PVP-NCMs.**

According to Table 4 (related to PVP-NCMs), and as expected from Fig. 6, PVP-NCM0.3 and PVP-NCM1.5 have the best behavior in water filtration with 14.9% decrease in membrane resistance. Considering total, cake and pore resistances, PVP-NCM1.5 has 30%, 4.6% and 50% resistance decrement, respectively. It can be concluded that even though the presence of 0.3 and 1.5 wt% ZnO nanoparticles in the membrane matrix creates similar effect on water filtration, greater loading of nanoparticles in PVP-NCM1.5 shows dramatic effects on humic acid filtration. Indeed, higher concentration of nanoparticles in PVP-NCM1.5 provides better fouling properties rather than PVP-NCM0.3, even though their membrane resistance is similar.

The performance of nanocomposite membranes in humic acid rejection was investigated. In Fig. 7, rejection of humic acid grows in the membrane for membranes containing up to 0.5% of nanoparticles. Thereafter, the greater the amount of nanoparticles, the lower the level of rejection, showing a decreasing trend. Indeed, PEG-NCM0.5 with a separation efficiency of 99.7% has the best performance in humic acid separation. The membrane containing a higher concentration than 0.5 wt% shows lower rejection efficiency which could be due to the increased amount of nanoparticles, their aggregation and pore plugging/clogging by accumulated nanoparticles and formation of individual large pores [15,48].

Unlike the research done by Junaidi et al. [12], PSF/ZnO nanocomposite membranes synthesized in this research had a better humic acid rejection, which amounts to 99.72%.

Humic acid rejection of PVP-NCMs is also presented in Fig. 7. The presented data shows that all nanocomposite membranes have a higher rejection than blank membrane. However, by adding different amount of nanoparticles to the casting solution, rejection of HA solution declined. Based on measurement of the mean pore size (Table 4) and SEM images (Fig. 3), the increment in the pore size could be the main cause of rejection loss.

## CONCLUSIONS

For better arrangement of ZnO nanoparticles around membrane pores, two categories of ZnO/PSf NCMs were synthesized through phase inversion method. Dope solution containing PEG

and dope solution containing PVP produced PEG-NCMs and PVP-NCMs, respectively. Surface, structural and functional investigation were conducted to find a better pore former and optimum nanoparticles' concentration. Membrane surface analysis was performed by AFM analysis and contact angle measurement. Based on AFM analysis, any increase in ZnO nanoparticles' concentration results in elevation of membrane roughness. Contact angle measurement confirms improved hydrophilicity of nanocomposite membranes. In structural evaluation, SEM analysis and porosity measurement both confirmed that PEG-NCMs are more porous than PVP-NCMs.

The filtration performance of PEG-NCMs in terms of pure water flux and humic acid rejection was evaluated, which introduced PEG-NCM0.5 as the membrane with a higher pure flux (503 LMH) and higher humic acid rejection (99.7%). Similarly, the filtration performance of PVP-NCMs was examined in which PVP-NCM0.3 offered the most acceptable performance in terms of pure water flux with a value of 245 LMH and humic acid rejection as large as 94.2%. Structural and performance investigation confirmed a positive effect of ZnO nanoparticles. It also emphasized that PEG-NCMs have a larger porosity, higher pure water flux and humic acid rejection than PVP-NCMs. This finding was also validated in resistance experiments in which 1.5 wt% ZnO nanoparticle decreased total filtration resistance for PEG-NCM1.5 and PVP-NCM1.5 by 89% and 30%, respectively. As a consequence, it is concluded that PEG has a better functionality as a pore former and to arrange ZnO nanoparticles.

## ACKNOWLEDGEMENTS

The authors would like to thank Professor Mehran Habibi Rezaei for his crucial assist and Iran Nanotechnology Initiative Council for supporting this investigation.

## NOMENCLATURE

A : effective area [$m^2$]
AFM : atomic force microscopy
CA : contact angle [°]
$C_f$ : humic acid concentration in feed solution [gr/lit]
$C_p$ : humic acid concentration in permeate solution [gr/lit]
HA : humic acid
J : output flux [$m^3/m^2s$]
$J_p$ : permeate flux [$m^3/m^2s$]
$J_s$ : humic acid solution flux [$m^3/m^2s$]
$J_{w1}$ : initial pure water flux [$m^3/m^2s$]
$J_{w2}$ : final pure water flux [$m^3/m^2s$]
l : membrane thickness [m]
NCM : nanocomposite membrane
NMP : N-methyl pyrrolidone
NOM : natural organic matter
PEG : polyethylene glycole
PES : polyethersulfone
PSF : polysulfone
PVA : polyvinyl alcohol
PVP : poly vinylpyrrolidone
Q : volumetric flow rate [$m^3/s$]
R : rejection [%]
$R_c$ : cake filtration resistance [$m^{-1}$]
$R_m$ : membrane filtration resistance [$m^{-1}$]
$R_p$ : pore filtration resistance [$m^{-1}$]
$r_p$ : pore radius [nm]
$R_t$ : total filtration resistance [$m^{-1}$]
RMS : root mean square roughness [nm]
SEM : scanning electron microscopy
TAP : 2,4,6-triaminopyrimidine
V : volume of membranein the wet state [$cm^3$]
$V_p$ : permeate volume [$m^3$]
$W_d$ : weight of dry membranes
$W_w$ : weight of wet membranes
zno : zinc oxide
$\Delta P$ : operational pressure [3 bar]
$\Delta P_t$ : pressure between the two side of embrane [Pa]
$\Delta_t$ : filtration duration [s]
$\rho_w$ : density of pure water flux at room temperature [$g/cm^3$]
$\varepsilon$ : porosity
$\varepsilon_{average}$ : average porosity
$\mu$ : viscosity of output solution [Pa·s]
$\eta$ : viscosity of water [$8.9*10^{-4}$ Pa·s]

## REFERENCES

1. A. I. Schäfer, A. G. Fane and T. D. Waite, Nanofiltration: Principles and applications, Elsevier (2005).
2. E. Trouve, V. Urbain and J. Manem, *Water Sci. Technol.*, **30**, 151 (2014).
3. A. K. Pabby, S. S. Rizvi and A. M. S. Requena, *Handbook of membrane separations: chemical, pharmaceutical, food, and biotechnological applications*, CRC Press (2015).
4. M. S. Muhamad, M. R. Salim and W.-J. Lau, *Korean J. Chem. Eng.*, **32**, 2319 (2015).
5. A. Hemmati, M. M. Dolatabad, F. Naeimpoor, A. Pak and T. Mohammdi, *Korean J. Chem. Eng.*, **29**, 369 (2012).
6. A. Asatekin, A. Menniti, S. Kang, M. Elimelech, E. Morgenroth and A. M. Mayes, *J. Membr. Sci.*, **285**, 81 (2006).
7. S. Liang, G. Qi, K. Xiao, J. Sun, E. P. Giannelis, X. Huang and M. Elimelech, *J. Membr. Sci.*, **463**, 94 (2014).
8. S. Liang, K. Xiao, Y. Mo and X. Huang, *J. Membr. Sci.*, **394-395**, 184 (2012).
9. K. Zodrow, L. Brunet, S. Mahendra, D. Li, A. Zhang, Q. Li and P. J. Alvarez, *Water Res.*, **43**, 715 (2009).
10. L. Li, Z. Zhao, W. Huang, P. a. Peng, G. Sheng and J. Fu, *Org. Geochem.*, **35**, 1025 (2004).
11. H.-J. Feng, L.-F. Hu, Q. Mahmood, Y. Long and D.-S. Shen, *Biochem. Eng. J.*, **39**, 478 (2008).
12. M. Junaidi, C. Leo, S. Kamal and A. Ahmad, *Water Sci. Technol.*, **67**, 2102 (2013).
13. J. Liu, Y. Song, R. Ruan and Y. Liu, *Water Sci. Technol.*, **72**, 92 (2015).
14. S. Bratskaya, S. Schwarz and D. Chervonetsky, *Water Res.*, **38**, 2955 (2004).
15. A. Ahmad, A. Abdulkarim, S. Ismail and B. Ooi, *Desalin. Water Treat.*, 1 (2014).

16. H. M. A. Asghar, S. N. Hussain, E. P. L. Roberts and N. W. Brown, *Korean J. Chem. Eng.*, **30**, 1415 (2013).
17. A. D. Levine, G. Tchobanoglous and T. Asano, *Journal (Water Pollution Control Federation)*, 805 (1985).
18. G. Leppard, D. Mavrocordatos and D. Perret, *Water Sci. Technol.*, **50**, 1 (2004).
19. N. Hamid, A. F. Ismail, T. Matsuura, A. Zularisam, W. J. Lau, E. Yuliwati and M. S. Abdullah, *Desalination*, **273**, 85 (2011).
20. I. Sutzkover-Gutman, D. Hasson and R. Semiat, *Desalin. Water Treat.*, **31**, 42 (2011).
21. J. Mansouri, S. Harrisson and V. Chen, *J. Mater. Chem.*, **20**, 4567 (2010).
22. J. Hong and Y. He, *Desalination*, **302**, 71 (2012).
23. S. Balta, A. Sotto, P. Luis, L. Benea, B. Van der Bruggen and J. Kim, *J. Membr. Sci.*, **389**, 155 (2012).
24. M. Homayoonfal, M. R. Mehrnia, S. Rahmani and Y. M. Mojtahedi, *J. Ind. Eng. Chem.*, **22**, 357 (2014).
25. M. Z. Yunos, Z. Harun, H. Basri, M. F. Shohur, M. R. Jamalludin and S. Hassan, *Jurnal Teknologi*, **65**(4), 111 (2013).
26. C.-P. Leo, W. Cathie Lee, A. L. Ahmad and A. W. Mohammad, *Sep. Purif. Technol.*, **89**, 51 (2012).
27. M. Homayoonfal, A. Akbari and M. R. Mehrnia, *Desalination*, **263**, 217 (2010).
28. M. R. Mehrnia, Y. M. Mojtahedi and M. Homayoonfal, *Desalination*, **372**, 75 (2015).
29. R. Derakhsheshpoor, M. Homayoonfal, A. Akbari and M. R. Mehrnia, *J. Env. Health Sci. Eng.*, **11**, 1 (2013).
30. B. Chakrabarty, A. K. Ghoshal and M. K. Purkait, *J. Membr. Sci.*, **315**, 36 (2008).
31. B. Chakrabarty, A. K. Ghoshal and M. K. Purkait, *J. Membr. Sci.*, **325**, 427 (2008).
32. M. Homayoonfal, M. R. Mehrnia, M. Shariaty-Niassar, A. Akbari, A. F. Ismail and T. Matsuura, *Desalination*, **354**, 125 (2014).
33. P. Woodward, First Ten Angstroms Inc., Portsmouth (1999).
34. S. Mafirad, M. Mehrnia and M. Sarrafzadeh, *Water Sci. Technol.*, **64**, 1154 (2011).
35. C. Liao, J. Zhao, P. Yu, H. Tong and Y. Luo, *Desalination*, **285**, 117 (2012).
36. J. F. Li, Z. L. Xu, H. Yang, C. P. Feng and J. H. Shi, *J. Appl. Polym. Sci.*, **107**, 4100 (2008).
37. I. Sadeghi, A. Aroujalian, A. Raisi, B. Dabir and M. Fathizadeh, *J. Membr. Sci.*, **430**, 24 (2013).
38. J.-F. Li, Z.-L. Xu, H. Yang, C.-P. Feng and J.-H. Shi, *J. Appl. Polym. Sci.*, **107**, 4100 (2008).
39. O. Agboola, J. Maree, R. Mbaya, C. M. Zvinowanda, G. F. Molelekwa, N. Jullok, B. Van der Bruggen, A. Volodine and C. Van Haesendonck, *Korean J. Chem. Eng.*, **31**, 1413 (2014).
40. N. Misdan, W. J. Lau, C. S. Ong, A. F. Ismail and T. Matsuura, *Korean J. Chem. Eng.*, **32**, 753 (2015).
41. M. Mulder, Basic Principles of Membrane Technology, Springer Science+Business Media Dordrecht, Netherlands (1996).
42. A. B. Koltuniewicz, R. Field and T. Arnot, *J. Membr. Sci.*, **102**, 193 (1995).
43. M.-J. Han and S.-T. Nam, *J. Membr. Sci.*, **202**, 55 (2002).
44. S. R. Panda and S. De, *J. Polym. Res.*, **20**, 1 (2013).
45. N. Brandes, P. B. Welzel, C. Werner and L. W. Kroh, *J. Colloid Interface Sci.*, **299**, 56 (2006).
46. M. Homayoonfal, M. R. Mehrnia, Y. M. Mojtahedi and A. F. Ismail, *Desalin. Water Treat.*, **51**, 3295 (2013).
47. M. Alhoshan, J. Alam, L. A. Dass and N. Al-Homaidi, *Adv. Polym. Technol.*, **32**(4), 21369 (2013).
48. P. Moradihamedani, N. A. Ibrahim, D. Ramimoghadam, W. M. Z. W. Yunus and N. A. Yusof, *J. Appl. Polym. Sci.*, **131**(16), 39745 (2014).
49. M. S. Gaur, P. K. Singh, Suruchi and R. S. Chauhan, *J. Therm. Anal. Calorim.*, **111**, 743 (2012).
50. A. Ismail and A. Hassan, *Sep. Purif. Technol.*, **55**, 98 (2007).
51. B. Chakrabarty, A. Ghoshal and M. Purkait, *J. Membr. Sci.*, **309**, 209 (2008).